

Dye reorientation as a probe of stress-induced mobility in polymer glasses

Hau-Nan Lee, Keewook Paeng, Stephen F. Swallen, and M. D. Ediger^{a)}*Department of Chemistry, University of Wisconsin-Madison, Madison, Wisconsin 53706, USA*

(Received 30 November 2007; accepted 25 January 2008; published online 3 April 2008)

The reorientation of dye molecules can be used to monitor the segmental dynamics of a polymer melt. We utilize this technique to measure stress-induced mobility in a lightly cross-linked poly(methyl methacrylate) (PMMA) glass during tensile creep deformation. At 377 K (18 K below the glass transition temperature T_g), the mobility increased by a factor of 100 during deformation with a stress of 20 MPa. Generally, the mobility increased as the stress, strain, and strain rate increased. After removing the stress, we observed that the enhanced mobility slowly disappeared during strain recovery. At 377 K, when the stress is lower than 11 MPa, almost no mobility enhancement was observed. Once the stress crossed this threshold value, the mobility dramatically increased. © 2008 American Institute of Physics. [DOI: 10.1063/1.2868774]

INTRODUCTION

Polymer glasses play an important role in technology and are gradually replacing other types of solids in many applications. Polymers can be processed into any desired shape with very low energy input and when cooled can form stiff solids. In contrast to other types of high modulus solids, polymer glasses are often tough, i.e., they can be deformed significantly without breaking. Even though polymer glasses are impressive engineering materials, current research seeks ways to enhance their modulus and toughness while maintaining ease of processing. This task requires the development of a fundamental understanding of the mechanisms that control the deformation of polymer glasses.^{1,2}

Yielding and plastic flow are key features in the deformation of polymer glasses and efforts to explain this behavior go back more than 70 years. In 1936, Eyring used his recently developed transition state theory to show that an applied stress acts to bias the potential energy curves that govern molecular rearrangements in viscous liquids and solids.³ He argued that the effective barrier height is lowered by an amount equal to the work done by the external force as a molecule (or polymer segment) crosses the barrier.

In broad terms, this view states that stress can transform a glass into a viscous liquid and yield can be viewed as the resulting viscous flow. Eyring predicted that the applied stress (σ) lowers the effective barrier linearly, and the transition rate (k_t) for structural rearrangements increases in an Arrhenius-like manner:

$$k_t = A \exp\left(-\frac{E_a - \sigma V}{k_B T}\right), \quad (1)$$

where $k_B T$ is the thermal energy, E_a is the barrier height when no stress is applied, V is a volume upon which the stress acts, and A is a prefactor.

Later workers have modified Eyring's approach in important ways while maintaining the central idea that stress

can induce mobility. In addition to the concepts introduced by Eyring, Robertson⁴ considered that stress might induce structural changes in a polymer glass. Robertson proposed a model that assumes that the shear stress changes the rotational conformations about backbone bonds and causes the fraction of flexed bonds (bonds with other than the preferred conformation) to increase. In this model, localized regions with an enhanced fraction of flexed bonds behave like a liquid because of the freer rotation of flexed bonds. Very recently, Chen and Schweizer⁵ proposed a statistical mechanical theory for stress-induced mobility in polymer glasses. This molecular-level approach is built upon a theory for segmental barrier hopping in polymer melts and glasses.^{6,7} The basic concept is that stress lowers the effective barriers for hopping by inducing an instantaneous force on a segment, but, in contrast to Eyring's model, the effective barriers decrease nonlinearly with the applied stress.

A few computer simulation studies have investigated changes in mobility in polymer glasses during nonlinear deformation. Capaldi *et al.*^{8,9} simulated amorphous polyethylene during compressive deformation and found that the conformational transition rates increased during periods of applied stress. Lyulin and co-workers^{10,11} studied the mobility of polystyrene (PS) and bisphenol A polycarbonate (PC) under uniaxial extension via molecular dynamics simulation. They observed, beyond the yield point, significant increases in the translational mobility of the PS and PC segments in the deformation direction. Recent simulations by Riggleman *et al.*¹² on a bead-spring polymer glass indicate that substantial mobility enhancements occur during both tensile and compressive deformation. This result, which contradicts simple free volume arguments, indicates a key connection between stress and mobility.

There have been several attempts to quantify stress-induced mobility in polymer glasses using mechanical measurements. In some of these experiments, a small strain is superposed on a large nonlinear deformation.^{13,14} If the response to the small deformation is interpreted as an experiment in the linear response regime, the mechanical relaxation

^{a)}Author to whom correspondence should be addressed. Electronic mail: ediger@chem.wisc.edu.

spectra are found to shift to shorter times as the overall deformation increases. These results have been interpreted as indicating that large strains and stresses can induce increased segmental mobility in polymer glasses. However, others have argued that this procedure is not rigorously justified and that these experiments have multiple possible interpretations.^{15,16}

Only recently experiments have directly investigated the response of molecular motions to the deformation of a polymer glass. Loo *et al.*¹⁷ used solid-state NMR to detect the mobility of the amorphous portions of a semicrystalline nylon 6 rod actively deformed inside a NMR probe. They reported an enhancement in mobility prior to yield. Zhou *et al.*¹⁸ demonstrated that the diffusion of resorcinol bis(diphenyl phosphate) into a poly(ether imide) glass under compression is similar to diffusion at much higher temperature without deformation. Watanabe *et al.*¹⁹ utilized a rheodielectric method to investigate an oligostyrene polymer melt well above the glass transition temperature T_g . They demonstrated that segmental motion is accelerated by shear flow.

In spite of these important efforts, a fundamental understanding of the nonlinear deformation behavior of glassy polymers has not yet been achieved. Part of what is missing is a quantitative understanding of how external stress speeds up segmental mobility in polymer glasses. An unambiguous experimental measurement that allows quantitative comparison to theory and simulation is required.

Here, we report the first optical measurements of stress-induced mobility in polymer glasses. A photobleaching method is used to measure the reorientation of a molecular probe in lightly cross-linked poly(methyl methacrylate) (PMMA) glass under stress. The reorientation of probes (on the time scale of seconds) has been previously shown to accurately monitor the segmental dynamics of polymer melts.^{20–22} Here, we utilize this method to quantitatively determine stress-induced mobility in a PMMA glass during tensile creep deformation.

We observe stress-induced mobility in PMMA glass at 377 K ($T_g - 18$ K). The largest change in mobility is about a factor of 100 (equivalent to a temperature increase of about 10 K in the glass). We observe higher segmental mobility as the strain and strain rates increase. After removing the stress, we observe that the enhanced mobility disappears slowly but completely. Additionally, the mobility enhancements are correlated with the true stress. When the stress is lower than 11 MPa, almost no mobility enhancement is observed. However, once the stress crosses this threshold value, the mobility increases significantly.

EXPERIMENTAL SECTION

Materials

A lightly cross-linked PMMA glass was utilized in this study. Cross-linking allows repeated measurements on a given sample since the effects of deformation can be erased by thermal cycling. The lightly cross-linked PMMA was synthesized using thermally initiated radical polymerization. The chemicals utilized in polymerization are methyl meth-

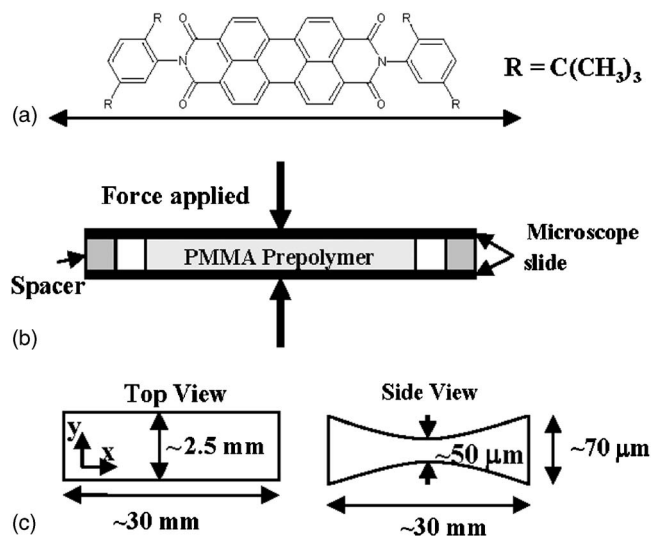


FIG. 1. (a) Chemical structure of *N,N'*-bis(2,5-di-*tert*-butylphenyl)-3,4,9,10-perylene-dicarboximide (BTBP). The arrow indicates the direction of the absorption transition dipole. (b) Mold for preparation of the PMMA film. (c) Dimensions of the test film and definition of coordinate system.

acrylate (MMA, monomer), ethylene glycol dimethacrylate (cross-linking agent), and benzoyl peroxide (initiator); these were obtained from Polysciences.

N,N'-bis(2,5-di-*tert*-butylphenyl)-3,4,9,10-perylene-dicarboximide (BTBP) was used as the molecular probe in the optical experiments and was supplied by Aldrich. The chemical structure of BTBP is shown in Fig. 1(a); here, the double-headed arrow shows the direction of absorption transition dipole.²³

Sample preparation

The synthetic procedure is briefly described as follows. A MMA solution containing 1.3% ethylene glycol dimethacrylate, 0.1% benzoyl peroxide, and $10^{-6}M$ BTBP was prepared. This solution was prepolymerized at 340 K for 30 min and then allowed to cool. The prepolymerization increased the viscosity of the mixture (making it easier to fill the mold) and, additionally, decreased the volume contraction during molding. The mold [Fig. 1(b)] consisted of two glass microscope slides, separated by aluminum foil spacers ($\sim 70 \mu\text{m}$), and held together with binder clips. After filling, the mold was clipped such that the force was directly applied at the center of the mold, so as to prepare PMMA films with curved sides, as shown in Fig. 1(c). The thicker portion of the specimen prevents the sample from breaking at the grip sites; deformation occurs primarily at the center of the film. The mold with PMMA prepolymer was placed in an oven purged with nitrogen (oxygen inhibits the free radical polymerization) at 340 K for 24 h. Finally, the temperature was increased to 395 K for an additional 24 h to eliminate residual monomer. After removal from the mold, the PMMA film was placed on a heated Teflon sheet and cut into $\sim 2.5 \times 30 \text{ mm}^2$ strips for optical and mechanical experiments. The thickness of the film was measured by a micrometer, and the width of the film was measured using a microscope. The sample T_g is 395 K as measured by differential scanning

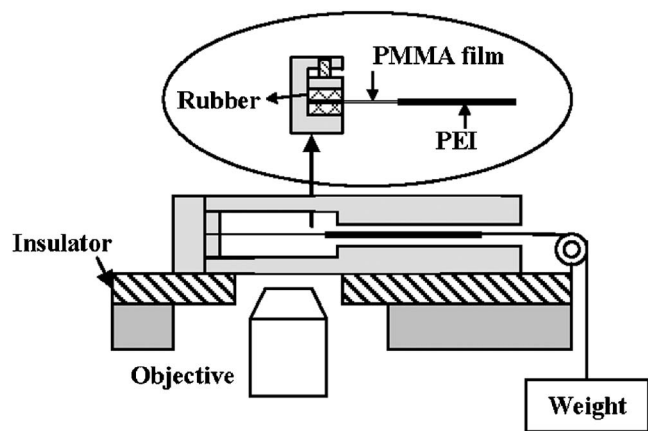


FIG. 2. Schematic of the creep apparatus. A freestanding PMMA film is placed in a temperature-controlled cell on a piezostage. The film is clamped between two rubber pieces at one end and glued between polyetherimide (PEI) sheets in another end. A constant stress is provided by a pulley and weight system. A window in the bottom of the cell allows light to pass between the microscope and the sample.

calorimetry (DSC) analysis (TA Instruments Q1000); this is the onset value obtained from the second heating scan at 10 K/min.

Deformation cell

Figure 2 shows a schematic image of our temperature-controlled deformation cell that allows simultaneous mechanical and optical measurements. A fused silica window attached to the bottom of the cell allows light to pass in and out of the microscope objective. Mechanical creep measurements were performed with a pulley and weight system linked to a freestanding PMMA film placed inside the cell. The entire deformation cell is mounted on a 3-axis piezoposition scanner (Mad City Labs, Nano-PDQ).

A Lake Shore model 330 temperature controller was used to measure the temperature of the cell and keep it constant to within ± 0.05 K. Four resistive cartridge heaters (Omega) were used to symmetrically heat the copper cell and a platinum resistance temperature detector (RTD) (Omega) placed directly above the PMMA film was used to measure the temperature. Another platinum RTD was placed near the open end of the cell. The temperature difference between the center and the end of the cell was within 0.3 K and we believe that the reported temperature accurately describes the film temperature to within 1 K.

Optical measurement of dye reorientation

A photobleaching method^{24,25} was used to measure BTBP reorientation in PMMA glasses. In these experiments, an intense linearly polarized beam is used to selectively photobleach dye molecules whose transition dipoles are aligned with the polarization of the light. This process creates an orientationally anisotropic distribution of unbleached dye molecules in the sample. Subsequently, the reorientation of the unbleached dye molecules regenerates an isotropic distribution. As we describe below, the time dependent anisotropy decay can be measured using the fluorescence from a weak

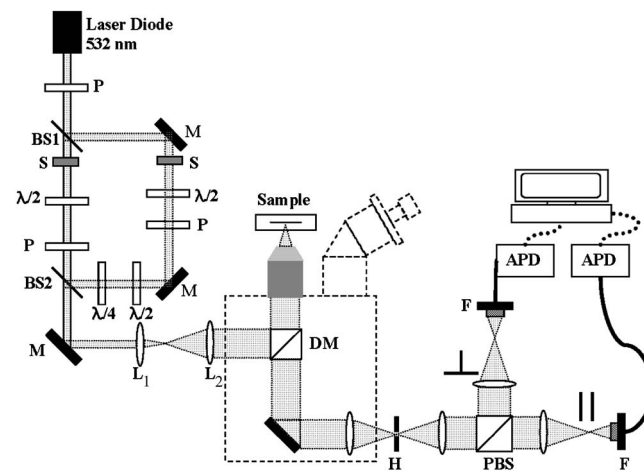
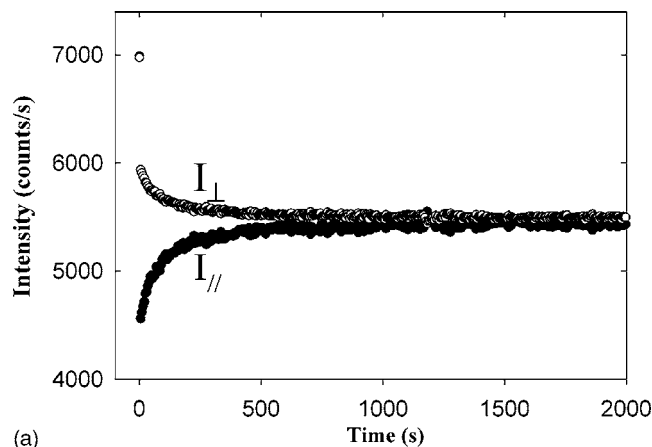


FIG. 3. Schematic of optical apparatus: *P*, polarizer; *S*, shutter; *M*, mirror; *BS*, beam splitter; *L*, lens; $\lambda/2$ ($\lambda/4$), half-(quarter-) wave retardation plate; *DM*, dichroic mirror; *H*, pinhole; *PBS*, polarizing beam splitter; *F*, fiber coupling; *APD*, avalanche photodiode. The dotted line indicates the Nikon TE2000 microscope.

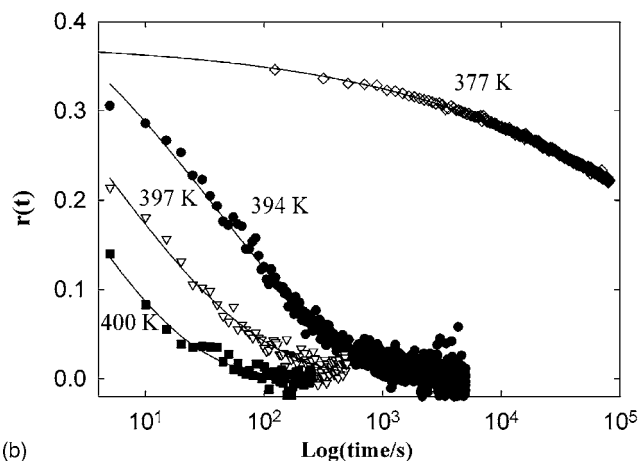
circularly polarized beam. We calculate the rotational correlation function and the rotational correlation time from the anisotropy decay function.

Figure 3 shows the confocal fluorescence microscope used for these measurements. A 532 nm light from a 30 mW continuous-wave diode laser passes through a beam splitter to form the bleaching and reading beams. The bleaching beam follows the direct path from BS1 to BS2 and has the following optical path: computer-controlled shutter, $\lambda/2$ wave plate for controlling the intensity of the bleaching beam at the sample, and a polarizer. The polarization of the bleaching beam is chosen to be parallel to the *y* axis [Fig. 1(c)] of the PMMA film. The reading beam follows the indirect path via two mirrors and has the following optical path: shutter, $\lambda/2$ wave plate, polarizer, another $\lambda/2$ wave plate, and $\lambda/4$ wave plate. We adjusted these optical components to control the intensity of the reading beam and make it circularly polarized at the sample. To verify that we have prepared circularly polarized light, we measured the ellipticity of the reading beam at the sample plane; with careful adjustment, we get the ratio of the light intensity in the parallel and perpendicular directions to be less than 1.15. The bleaching and reading beams follow the same optical path after BS2. After being expanded, they are delivered to the epi-illumination port of the microscope, and then are focused to a $1 \mu\text{m}$ spot by the objective (Nikon Plan Fluor, 10 \times , numerical aperture=0.3). The fluorescence light is collected with the same objective. The path of the fluorescence photons in the body of the microscope consists of a dichroic mirror and emission filter (for excitation rejection) and the tube lens. After passing through the pinhole, which defines the collection plane in the sample, the emission light is directed to a polarizing beam-splitter cube that is used to project the two orthogonally polarized emission components onto two avalanche photodiodes. LABVIEW programs are used for device control and data acquisition.

Figure 4 shows photobleaching measurements of BTBP reorientation in PMMA in the absence of deformation. In the



(a)



(b)

FIG. 4. (a) Photobleaching measurements of BTBP reorientation in undeformed PMMA at 394 K. (●) Fluorescence intensity for polarization parallel to the bleaching beam polarization. (○) Fluorescence intensity (after being multiplied by the g factor) for polarization perpendicular to the bleaching beam polarization. (b) Anisotropy $r(t)$ decays for BTBP in undeformed PMMA at the temperatures indicated. The solid lines are KWW fits to the data.

remainder of this section, we describe how these data were obtained and analyzed. A photobleached pattern (Fig. 5, lower left) was created by the intense linearly polarized bleaching beam for the dye reorientation measurement. Immediately after photobleaching ($t=0$), the circularly polarized reading beam was introduced to induce fluorescence from the area inside the photobleached pattern. The time dependent fluorescence intensities for polarization parallel $I_{\parallel}(t)$ and perpendicular $I_{\perp}(t)$ to the bleaching beam polarization are shown in Fig. 4(a). The excitation beam preferentially photobleaches the probe molecules whose absorption transition dipoles are aligned with the polarization of the beam. Therefore, an orientationally anisotropic distribution of transition dipoles is created, and $I_{\parallel}(0)$ is weaker than $I_{\perp}(0)$. In time, the unbleached dye molecules reorient to regenerate an isotropic distribution of the transition dipoles, and then the fluorescence intensities from both polarizations become identical.

The fluorescence intensities shown in Fig. 4(a) are corrected for the efficiencies of the APDs, the polarization changes caused by the optical components, and the imperfection of the circularly polarized reading beam. We obtained a correction factor g by illuminating an unbleached portion of

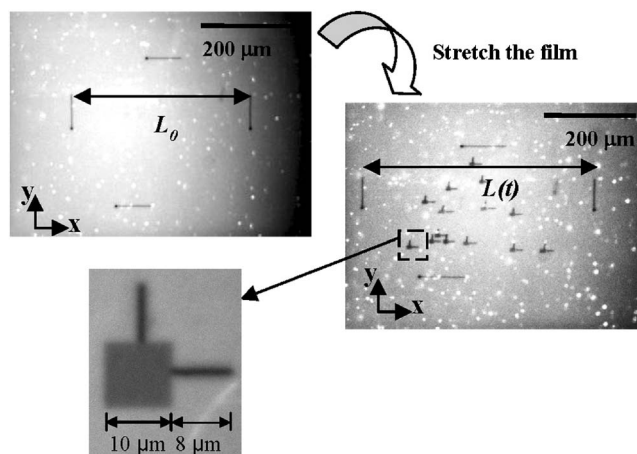


FIG. 5. Local measurement of strain and BTBP reorientation. The four photobleached lines define the region where local strain and mobility measurements are performed. The local strain is defined as $\varepsilon(t) = (L(t) - L_0) / L_0$. The small bleach patterns are used for measurements of BTBP reorientation; one of these regions is shown in detail in the lower left. These images were obtained with wide field illumination; photobleached regions appear dark because less fluorescence originates from these regions.

the sample with circularly polarized light and measuring the ratio of fluorescence intensities for two emission polarizations, $I_{\parallel}^{\text{un}} / I_{\perp}^{\text{un}}$. For undeformed samples, g is in the range of 1.10–1.20. The fluorescence intensity perpendicular to the bleaching beam $I_{\perp}(t)$ is multiplied by this g factor before further analysis.

Figure 4(b) shows the anisotropy decay function $r(t)$ measured at four different temperatures. $r(t)$ is defined by the following equations:

$$r(t) = \frac{\Delta I_{\parallel}(t) - \Delta I_{\perp}(t)}{\Delta I_{\parallel}(t) + 2\Delta I_{\perp}(t)}, \quad (2)$$

$$\Delta I_{\parallel}(t) = I_{\parallel}^{\text{un}}(t) - I_{\parallel}(t), \quad (3)$$

$$\Delta I_{\perp}(t) = gI_{\perp}^{\text{un}}(t) - gI_{\perp}(t). \quad (4)$$

Here, $\Delta I_{\parallel}(t)$ is the difference in the parallel fluorescence intensity between an unbleached part of the sample and the bleached part of the sample at time t after bleaching; $\Delta I_{\perp}(t)$ is defined analogously. In order to correct for fluorescence intensity fluctuations caused by laser power fluctuations, we modify Eqs. (3) and (4) to get Eqs. (5) and (6). All the $r(t)$ decay curves shown in this work were calculated using Eqs. (2), (5), and (6).

$$\Delta I_{\parallel}(t) = I_{\parallel}^{\text{un}}(t) - I_{\parallel}(t) \frac{I_{\parallel}^1 + 2gI_{\perp}^1}{I_{\parallel}(t) + 2gI_{\perp}(t)}, \quad (5)$$

$$\Delta I_{\perp}(t) = gI_{\perp}^{\text{un}}(t) - gI_{\perp}(t) \frac{I_{\parallel}^1 + 2gI_{\perp}^1}{I_{\parallel}(t) + 2gI_{\perp}(t)}. \quad (6)$$

Here, I_{\parallel}^1 and I_{\perp}^1 are the first fluorescence intensity data collected after photobleaching.

The orientation autocorrelation function $CF(t)$ can be obtained from the anisotropy function $r(t)$ by

$$CF(t) = r(t)/r(0). \quad (7)$$

The orientation autocorrelation function is related to molecular reorientation by

$$CF(t) = \langle P_2[\hat{\mu}(0) \cdot \hat{\mu}(t)] \rangle. \quad (8)$$

Here, $\hat{\mu}$ is the absorption dipole for the BTBP molecule, P_2 is the second Legendre polynomial, and the brackets represent an ensemble average. The data in Fig. 4(b) have been fitted with the stretched exponential function [Kohlrausch–Williams–Watts (KWW) function]

$$CF(t) = e^{-(t/\tau)^\beta}. \quad (9)$$

The integral of the correlation function provides the rotational correlation time τ_c , which is given by

$$\tau_c = \int_0^\infty CF(t) dt = \frac{\tau}{\beta} \Gamma(1/\beta), \quad (10)$$

where Γ is the gamma function.

Local creep measurement

Uniaxial tensile creep has been used to deform the PMMA films. The creep experiments measure the elongation of the PMMA films subjected to a constant load at constant temperature. The engineering stress σ_0 is held constant during a creep measurement and is defined as $\sigma_0 = F/A_0$, where F is the applied force and A_0 is the original (undeformed) cross-sectional area [$\sim 0.125 \text{ mm}^2$, see Fig. 1(c)]. The results of the creep measurements are expressed as the local strain as a function of time, which is defined as $\varepsilon(t) = (L(t) - L_0)/L_0$. Here, L_0 is the initial length of some small section of the sample and $L(t)$ is the length at time t .

Figure 5 illustrates how the local strain was measured. Four lines created by photobleaching define the region ($\sim 400 \times 400 \mu\text{m}^2$) where the local strain and mobility measurements are made. Monitored by a charge coupled device (CCD) camera, the increase of distance between the two lines perpendicular to the direction of deformation (x axis) determined $\varepsilon(t)$, while the decrease of distance between the two lines parallel to the direction of deformation determined the transverse contraction of the PMMA film. As described below, mobility measurements were made inside the region described by these parallel lines. This method allows us to unambiguously determine the strain in the region where the mobility measurements are performed. Since L_0 is only about $400 \mu\text{m}$ and no distortion of the bleached lines was observed, we can safely assume that in the region where the measurements were conducted, the sample deformed homogeneously.

The true stress is defined as the ratio of the applied force (F) to the instantaneous cross-sectional area (A). Since A is decreasing as the sample is elongated, the true stress increases as the strain increases. To obtain the instantaneous area experimentally, we monitored the local change in width with the CCD camera (i.e., the distance between the two lines parallel to the x axis in Fig. 5). For one sample, we measured the fractional change in total width of the PMMA film and found that it was identical to the local contraction in

width. Thus, we assume that our samples deform uniformly in the yz plane and use the measured contraction in the y direction for both the y and z directions. Based on this information, we can calculate the instantaneous cross-sectional area (A) and the true stress.

To get consistent results, the film was heated to 400 K for 3 h to remove any residual stress in the film. We then cooled the film to the testing temperature and waited until the temperature was stable. The total cooling and waiting time prior to the mechanical experiments was 30 min.

Optical measurement of dye reorientation during deformation

We measured dye reorientation by photobleaching a pattern on the sample that included a $10 \times 10 \mu\text{m}^2$ square pattern and two $8 \mu\text{m}$ lines (Fig. 5, lower left corner). During deformation, the photobleached pattern moves along the direction of elongation. In order to track the pattern, we use the piezopositioner to drive the deformation cell in the opposite direction of the deformation. By scanning across the two $8 \mu\text{m}$ lines, the center position of the square pattern could be accurately located.

Since the optical measurements were done in a confocal geometry (defined by the pinhole in Fig. 3), we only collect fluorescence from the center $10 \mu\text{m}$ of the $50 \mu\text{m}$ thick film. During the deformation, we also scan the piezopositioner across the z axis to ensure that we measure mobility in the center of the film.

Correction for the alignment of probe molecules

The ratio of $I_{\parallel}^{\text{an}}$ to I_{\perp}^{an} ($\equiv g$) is constant when the strain is small. We found that the g factor decreased from 1.10 to 0.90 as the strain increased to $\sim 60\%$, indicating that the probe molecules in the PMMA film become aligned as the film is deformed; even larger strains (165%) lowered g to 0.70. Consistent with the work of Michl *et al.*,²⁶ the long axis of BTBP is found to align in the direction of the deformation. In order to account for the influence of this alignment on the anisotropy decay, further manipulation of the fluorescence intensities is necessary. Therefore, we replaced the g factor used in Eqs. (5) and (6) by a time dependent correction factor $g(t) = I_{\parallel}^{\text{an}}(t)/I_{\perp}^{\text{an}}(t)$.

To test the validity of this correction, we performed two matched anisotropy measurements during deformation. The experiments were identical except that the bleaching beam polarization was parallel to the x axis (the extension axis) of the PMMA film in one case and parallel to the y axis in the other. During this experiment, $g(t)$ changed by 40%. If a time independent g factor is used in the data analysis, the two $r(t)$ decay curves differ significantly from each other because probe alignment affects the two experiments in opposite ways; alignment either increases $I_{\parallel}(t)$ at the expense of $I_{\perp}(t)$, or vice versa. If $g(t)$ is used to analyze the data, the two $r(t)$ decay curves are identical within the experimental error, as shown in Fig. 6. We regard this result as experimental evidence that use of $g(t)$ removes the influence of probe alignment from the experimental data.

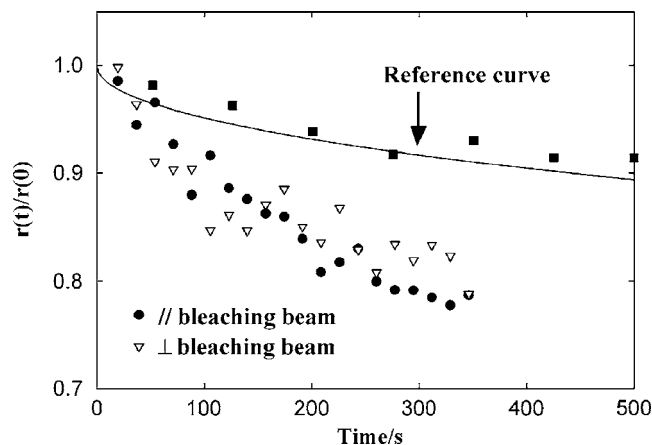


FIG. 6. Test of correction scheme for dye alignment. (●) Anisotropy decay $r(t)$ for BTBP in PMMA during deformation using a bleaching beam polarized along the y axis. (▽) Anisotropy decay $r(t)$ for BTBP in PMMA during deformation using a bleaching beam polarized along the x axis. (■) Anisotropy decay $r(t)$ for BTBP in undeformed PMMA as a reference; the solid line is a KWW fit to the data. After applying the $g(t)$ correction described in the text, the two anisotropy decay curves are identical within experimental error.

RESULTS

Temperature dependence of rotational correlation times

Figure 7 shows the rotational correlation times for dilute BTBP in PMMA at different temperatures with no applied stress. These values were obtained by fitting data similar to that shown in Fig. 4. The solid curve in Fig. 7 above T_g is the temperature dependence of the dielectric relaxation time τ_{or} ²⁷ vertically shifted to match the BTBP rotational correlation times. The rotational correlation times of BTBP follow the temperature dependence of the dielectric relaxation time very well above T_g . This indicates that the reorientation of this probe molecule is strongly correlated with the segmental dynamics of PMMA. This result is consistent with work done previously by Ediger and co-workers on other polymers.^{20–22} They showed that the reorientation of the dye

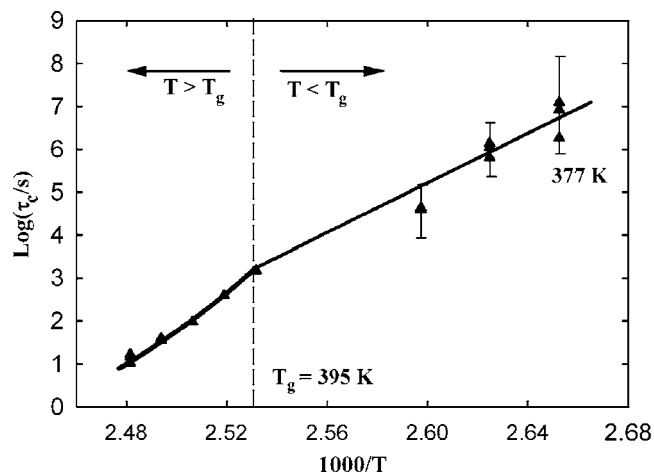


FIG. 7. Rotational correlation times for BTBP in undeformed PMMA at different temperatures. The solid curved line above T_g is the temperature dependence of the dielectric relaxation time from Ref. 27, shifted vertically. The solid straight line below T_g is a guide to the eye.

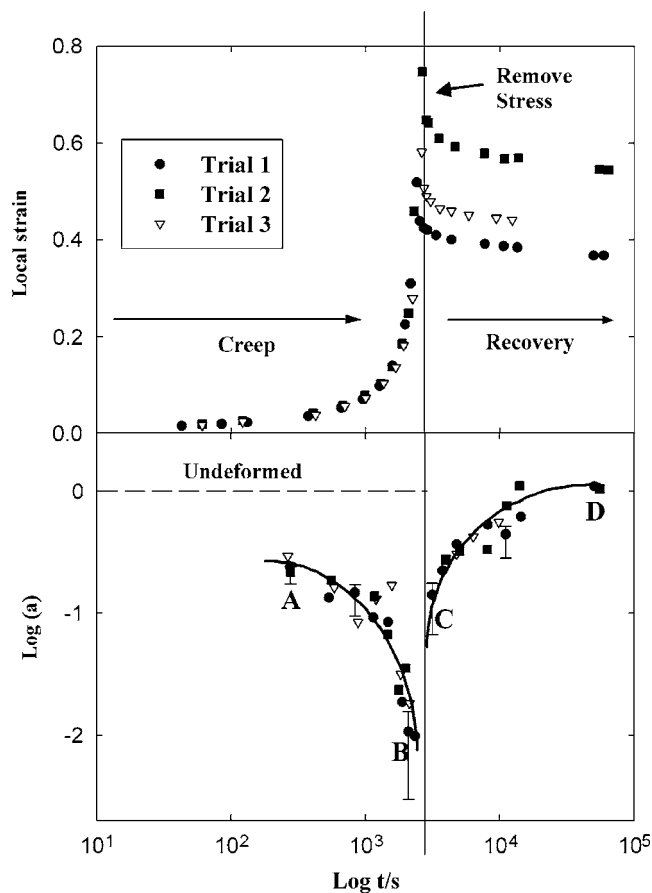


FIG. 8. (a) Three trials of creep and recovery experiments on PMMA at 377 K with an engineering stress of 15.8 MPa. (b) Shift factor for the rotational correlation time, showing a hundredfold increase in mobility during creep. The solid lines are guides to the eye. The labels A, B, C, and D, refer to Fig. 9.

molecules can be used to monitor the segmental dynamics of a polymer melt as long as the dye is not too small. Based on this result, we assume that the rotational correlation times of the probe molecule are also strongly correlated with the segmental dynamics of a polymer during deformation below T_g .

For the data shown in Fig. 7 below T_g , we did not observe the complete anisotropy decay. We performed long anisotropy measurements to get as much of $r(t)$ as possible, as shown for the 377 K data in Fig. 4. With a 1 day experiment, we observed about 40% of the anisotropy decay. In all cases, we fit $r(t)$ to the KWW function to obtain the rotational correlation time. At 377 K, in the absence of deformation, $\tau_c \approx 10^7$ s with $\beta \approx 0.4$. As the data were collected at 377 K, physical aging was occurring and the mobility was decreasing over the course of the measurement. If this effect could be taken out of the data, the anisotropy function would decay faster at long times and the β value would be larger. The solid straight line below T_g in Fig. 7 is a guide to the eye. As expected, there is a discontinuity in slope at $T \approx T_g$ as the results below T_g are for nonequilibrium glass samples.^{6,28,29}

Changes in rotational correlation times with stress

Figure 8 shows three trials of creep and BTBP reorientation measurements at 377 K ($T_g - 18$ K) with engineering stress equal to 15.8 MPa. During each creep experiment, we

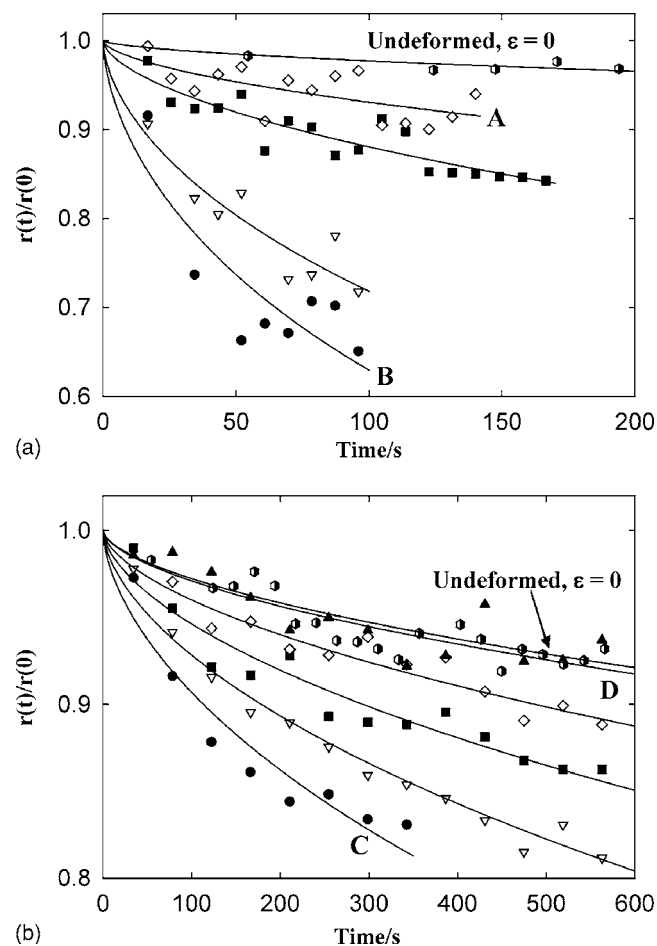


FIG. 9. (a) Normalized anisotropy decays obtained during the creep experiment shown in Fig. 8(a). These curves were obtained from photobleaching experiments starting 206 s (\diamond), 1060 s (\blacksquare), 1836 s (∇), and 2037 s (\bullet) after applying the stress. (b) Normalized anisotropy decays obtained during recovery. Curves obtained at 2955 s (\bullet), 3438 s (∇), 4456 s (\blacksquare), 14020 s (\diamond), and 50235 s (\blacktriangle) after applying the stress. The A, B, C, and D anisotropy decay curves were performed at times A, B, C, and D in Fig. 8(b). The solid lines are KWW fits to the data. During creep, from time A to time B, as strain and strain rate increase, higher mobility (faster anisotropy decays) is observed. After removing the stress, the enhanced mobility slowly disappears.

performed about eight optical experiments to measure the mobility of the polymer at different strain levels. Some of the anisotropy decay functions for one trial are shown in Fig. 9. This method allows us to monitor the mobility of the polymer glass at multiple times (and strain levels) during deformation. A consequence of this method is that we only obtain the initial portion of the anisotropy decay in each mobility measurement.

As shown in Fig. 9(a), as the strain and strain rates increase, we observe faster $r(t)$ decays indicating higher mobility. After removing the stress, we observe slower $r(t)$ decays as the strain recovers, as shown in Fig. 9(b). To quantitatively analyze the mobility change during creep and recovery experiments, we fit the anisotropy decay curves to the KWW function. Since we observe only a small portion of the anisotropy decay, an unconstrained fit with the KWW function does not yield reliable parameters. Instead, we used information from mobility measurements with no applied stress to estimate the KWW β parameter during deformation.

We assume that β does not have an intrinsic temperature dependence²² and that the shape of the anisotropy decay function does not change due to deformation. Thus, we fit $r(t)$ to the KWW function by keeping β fixed at 0.6, the value for BTBP rotation in PMMA just above T_g . Similarly, we fit the initial portion of $r(t)$ for the undeformed sample with β constrained to 0.6. We consider this fitting procedure to yield a good estimate of the shift factor $a = \tau_c(\text{deformed}) / \tau_c(\text{undeformed})$. The absolute τ_c values obtained from these KWW fits likely have less significance.

Figure 8(b) shows the logarithmic shifts $[\log(a)]$ of the rotational correlation times for BTBP molecules in PMMA during deformation. As the strain and strain rate increase, we observe higher mobility. The largest change in mobility is about a factor of 100. This is equivalent to a temperature increase of about 10 K, as shown in Fig. 7, but this mobility enhancement results from the applied stress and not an actual temperature increase. Immediately after removing the stress, the mobility decreases significantly, and then disappears slowly but completely. Note that no mobility enhancement was observed after $\sim 10^5$ s, even though the total strain is still very high. Also note that the three runs have very similar changes in mobility during recovery, even though the strain values are significantly different.

To test the reproducibility of these results, the measurements have been repeated three times under the same conditions, as shown in Fig. 8. For these experiments, we did not remove the stress at exactly the same time. Since the strain rate is very large at this phase of the experiment, a few seconds time difference result in a large strain difference. Within our experimental error, we observed the same mobility enhancement as a function of time in the three experiments.

In the above analysis, we assumed that the β value in the KWW function is independent of temperature over a 20 K temperature range. We fit $r(t)$ at $T_g - 18$ K with β constrained to 0.6, the value for BTBP rotation in PMMA just above T_g . To test the impact of this assumption, we also fit $r(t)$ to the KWW function while keeping β fixed at two additional values. The largest β that we have obtained for this system near T_g was 0.67, which we set as an upper bound for β at $T_g - 18$ K. The β obtained by fitting $r(t)$ for $T_g - 18$ K [Fig. 4(b), data at 377 K] was 0.4, which we regard as a lower bound for the β value since aging acts to stretch the anisotropy curve during acquisition in the glass. We recalculated $\log(a)$ using the procedure above and these two values of β in the KWW fits; these results are shown for some points as error bars in Fig. 8. As indicated by the figure, varying β has an impact on the shift factor but this impact is not much larger than our run-to-run variations. Thus, within reasonable bounds, particular assumptions about the KWW β parameter below T_g do not have a major impact on the interpretation of our data. We anticipate that improvement in our signal-to-noise ratio in the anisotropy measurements will allow us to refine our assumptions about the KWW β .

For comparison, we performed additional measurements with a lower stress level (11 MPa), as shown in Fig. 10. No significant mobility enhancement was observed. The correlation times actually increase at later times in this experiment,

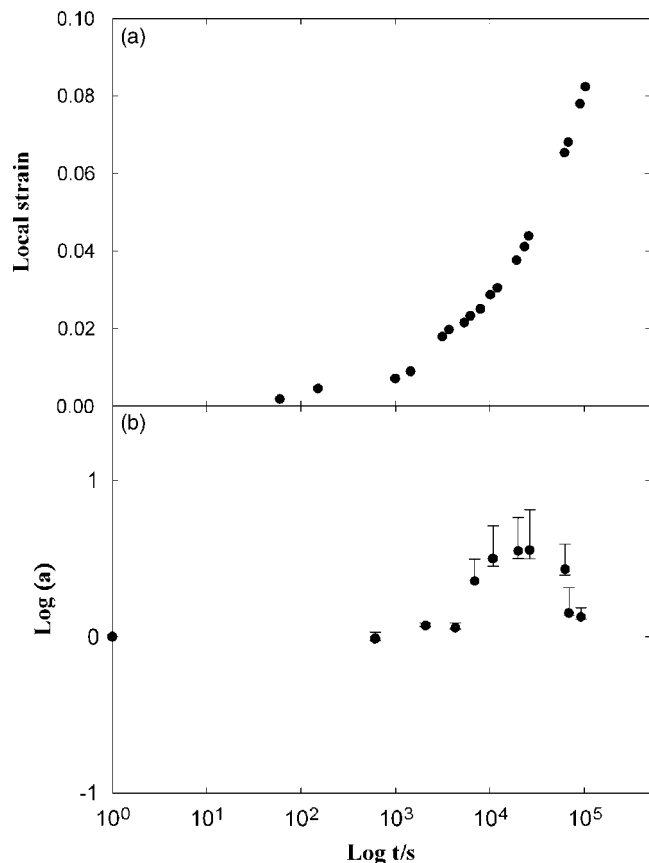


FIG. 10. (a) Creep experiment on PMMA at 377 K with an engineering stress of 11.0 MPa. (b) Shift factor for the rotational correlation time. Very little change in mobility is observed.

likely due to physical aging. We performed a control experiment similar to that shown in Fig. 10 except that the sample was not deformed; no mobility change occurred up to 10^4 s and a slowing of mobility by 0.2 decades was observed between 10^4 and 10^5 s. We interpret this control experiment to mean that physical aging can account for the slowing of dynamics in Fig. 10 and that physical aging has essentially no impact on the increase in mobility shown in Fig. 8.

In order to compare our results with theoretical models^{3,5} that predict that the applied stress increases mobility in a polymer glass, we plot the logarithmic shifts of the correlation times as a function of true stress in Fig. 11. Figure 11 shows that mobility enhancements are correlated with the true stress during deformation at 377 K. When the true stress is lower than ~ 11 MPa, essentially no mobility enhancement is observed. However, once the true stress crosses this threshold value, the mobility increases dramatically. Qualitatively this form of stress dependence had been shown in the work done by Schapery.³⁰ He found that the shear stress accelerates the time dependent part of the creep response in a fiber-reinforced phenolic resin and this acceleration only occurs after a critical shear stress is reached. Note that we do not claim that the mobility of polymer glasses during deformation is only a function of the true stress. Other variables such as strain rate or yield behavior may also have an important, independent impact on mobility of polymer glasses.

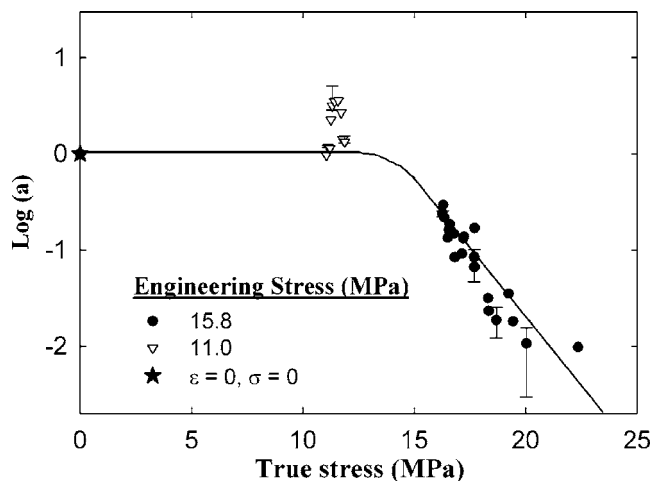


FIG. 11. The shift factor for the rotational correlation time as a function of the true stress for PMMA at 377 K.

DISCUSSION

The results presented above demonstrate that the segmental mobility of polymeric glasses is enhanced dramatically when the glasses are subjected to large levels of stress. The combination of local measurements of mobility and strain provide unambiguous results that allow a quantitative comparison to theory and simulation.

Comparison to NMR experiments of Loo *et al.*¹⁷

Direct experimental measurements of stress-induced mobility on a deformed semicrystalline polymer have been reported by Loo *et al.* They performed NMR measurements on a nylon 6 rod as it was being deformed inside a NMR probe. They recorded solid-state NMR line shapes that are sensitive to molecular mobility. By analyzing the changes in the NMR line shapes, changes in the molecular mobility were qualitatively determined. In their experiments, the nylon 6 rod was stretched with constant strain rate to a strain of 0.36 at 1 K above T_g ; then a stress relaxation experiment was conducted with the specimen held at constant length for 1 h, and then a constant strain rate deformation was resumed. The mobility associated with the amorphous region (where the deformation occurs) was found to increase with strain and to decrease as the specimen was allowed to relax. When the deformation was resumed, the stress and mobility both increased. Loo *et al.* did not report quantitative values for the extent to which mobility is enhanced, but qualitatively the change in polymer mobility during deformation in this NMR experiment is consistent with our measurements. Both experiments indicate a strong correlation between stress and mobility. However, in our experiments, in order to get a measurable mobility enhancement, the applied true stress had to be larger than a threshold value. This feature was not reported by Loo *et al.* but this may be due to differences in the experimental conditions. Loo *et al.* performed a constant strain rate mechanical experiment on a semicrystalline polymer at 1 K above T_g , while we used a creep experiment on an amorphous polymer glass at 18 K below T_g .

Comparison to purely mechanical measurements

As mentioned in the Introduction, purely mechanical measurements have been used to infer changes in mobility of polymer glasses during deformation.^{13,14} Martinez-Vega *et al.*,¹³ for example, combined a low stress torsional creep experiment with a high extensional stress in a study of PMMA. At $T_g - 15$ K, with an engineering stress of 8.2 MPa, the relaxation spectrum associated with torsion shifted to shorter times as the tensile deformation increased. The largest apparent decrease in relaxation time was about a factor of 35. Once the stress was removed, the apparent relaxation time slowly increased. When the applied stress was 4.1 MPa, the relaxation times associated with torsion did not change with the extensional deformation. The analysis of Ref. 13 is based on the assumption that the small torsional creep is not coupled to the large tensile deformation and can be interpreted in the linear response regime. Under this assumption, these results are qualitatively similar to what we report here. However, as pointed out by McKenna and Zapas,¹⁶ there is no rigorous justification for this assumption, and other interpretations are possible. Using our optical technique, we directly observe changes in molecular mobility during deformation. It would be useful to do a direct comparison of the optical experiments with a mechanical deformation measurement similar to the design of Ref. 13.

An important feature of our experiment is that we measure the mobility locally in the deformed specimen, while a standard mechanical measurement probes the response of the whole specimen. When the deformation is large, glassy samples deform inhomogeneously. In this regime, mechanical methods can only provide some average of the mobility in regions with different strains and true stresses. In contrast, we locally measure the strain, stress, and strain rate, as well as the molecular mobility. In principle, we should be able to simultaneously measure mobility changes in different parts of an inhomogeneously deformed sample.

Comparison to theory and simulation

An early theory developed by Eyring³ postulated that applied stress induces molecular mobility by lowering the energy barrier for localized rearrangements such as segmental movement. This model predicts that stress (σ) lowers the effective barrier linearly and thus the logarithm of the structural relaxation time $\ln \tau_\alpha$ decreases linearly with the applied stress:

$$\ln \tau_\alpha = \frac{E_a}{K_B T} - \frac{\sigma V}{K_B T} - \ln A. \quad (11)$$

This prediction would be a straight line in the format of Fig. 11 and thus is qualitatively inconsistent with the experimental data.

Chen and Schweizer⁵ developed a predictive theory for stress-enhanced mobility in polymer glasses built upon a theory of segmental barrier hopping. In contrast to the Eyring model, the barriers for hopping decrease in a nonlinear manner with the stress. Using this information, Chen and Schweizer predicted segmental relaxation times as a function of stress for PMMA glasses. For conditions comparable to

our experiment, with a stress of 20 MPa, they predict that the relaxation time drops by about two orders of magnitude, which is similar to our experimental result. However, the dependence of molecular mobility on stress is different than in Fig. 11. Their predictions illustrate a smooth dependence of the mobility on stress while Fig. 11 indicates that the stress apparently has to be larger than a threshold value to induce a significant mobility enhancement.

Recently, Riggleman *et al.*¹² employed molecular dynamics computer simulations to study stress-induced mobility of a polymer. They found that mobility increases of about two orders of magnitude during both tensile and compressive deformation. They argued that changes in free volume cannot explain this mobility enhancement, since they observed mobility enhancement during compression even though the volume decreased during this simulation. They found that the logarithm of mobility increased faster than linearly with stress, in qualitative agreement with Fig. 11.

CONCLUSIONS

We have built an optical apparatus to measure stress-induced mobility of polymer glasses. At 18 K below T_g , a factor of 100 increase in mobility was observed. Generally, mobility increased as the stress, strain, and strain rates increased. After removing the stress, we observed that the enhanced mobility slowly disappeared, even though the overall strain was still very large. In addition, mobility enhancements were correlated with true stress during creep. When the stress was lower than ~ 11 MPa, almost no mobility enhancement was observed. Once the stress crossed this threshold value, the mobility rose dramatically.

A large number of factors potentially influence how deformation changes mobility in polymer glasses, including stress, strain rate, temperature, and thermal history. Future experiments will aim to determine whether all these factors are independent or whether a simpler description of this phenomenon might be possible. We will further investigate the apparent threshold stress required for mobility enhancement. Understanding how mobility changes in different parts of an inhomogeneously deformed glass is also interesting. In addition, experiments on PMMA/silica nanocomposites are being initiated. Nanoscale fillers can transform brittle polymer glasses into ductile materials. We are eager to use measurements of stress-induced mobility to probe the microscopic mechanisms of this nanoscale filler effect.

ACKNOWLEDGMENTS

This work was supported by the National Science Foundation (No. NIRT 0506840). We thank Jim Caruthers for stimulating our interest in this problem and for suggesting that optical measurements of probe rotation might show large changes with deformation. We thank Ken Schweizer, Juan de Pablo, Rob Riggleman, Jim Caruthers, and Grigori Medvedev, for useful discussions. We thank Lian Yu and Ye Sun for performing DSC measurements.

¹D. B. Adolf, R. S. Chambers, and J. M. Caruthers, *Polymer* **45**, 4599 (2004).

²J. M. Caruthers, D. B. Adolf, R. S. Chambers, and P. Shrikhande,

- Polymer* **45**, 4577 (2004).
- ³H. Eyring, *J. Chem. Phys.* **4**, 283 (1936).
- ⁴R. E. Robertson, *J. Chem. Phys.* **44**, 3950 (1966).
- ⁵K. Chen and K. S. Schweizer, *Europhys. Lett.* **79**, 26006 (2007).
- ⁶K. Chen and K. S. Schweizer, *J. Chem. Phys.* **126**, 014904 (2007).
- ⁷K. S. Schweizer and E. J. Saltzman, *J. Chem. Phys.* **121**, 1984 (2004).
- ⁸F. M. Capaldi, M. C. Boyce, and G. C. Rutledge, *Polymer* **45**, 1391 (2004).
- ⁹F. M. Capaldi, M. C. Boyce, and G. C. Rutledge, *Phys. Rev. Lett.* **89**, 175505 (2002).
- ¹⁰A. V. Lyulin, N. K. Balabaev, M. A. Mazo, and M. A. J. Michels, *Macromolecules* **37**, 8785 (2004).
- ¹¹A. V. Lyulin, B. Vorselaars, M. A. Mazo, N. K. Balabaev, and M. A. J. Michels, *Europhys. Lett.* **71**, 618 (2005).
- ¹²R. A. Riggleman, H. Lee, M. D. Ediger, and J. J. De Pablo, *Phys. Rev. Lett.* **99**, 215501 (2007).
- ¹³J. J. Martinez-Vega, H. Trumel, and J. L. Gacougnolle, *Polymer* **43**, 4979 (2002).
- ¹⁴A. F. Yee, R. J. Bankert, K. L. Ngai, and R. W. Rendell, *J. Polym. Sci., Part B: Polym. Phys.* **26**, 2463 (1988).
- ¹⁵G. B. McKenna, *J. Phys.: Condens. Matter* **15**, S737 (2003).
- ¹⁶G. B. McKenna and L. J. Zapas, *Polym. Eng. Sci.* **26**, 725 (1986).
- ¹⁷L. S. Loo, R. E. Cohen, and K. K. Gleason, *Science* **288**, 116 (2000).
- ¹⁸Q. Y. Zhou, A. S. Argon, and R. E. Cohen, *Polymer* **42**, 613 (2001).
- ¹⁹H. Watanabe, Y. Matsumiya, and T. Inoue, *J. Phys.: Condens. Matter* **15**, S909 (2003).
- ²⁰C. Y. Wang and M. D. Ediger, *Macromolecules* **30**, 4770 (1997).
- ²¹Y. Hwang and M. D. Ediger, *J. Polym. Sci., Part B: Polym. Phys.* **34**, 2853 (1996).
- ²²T. Inoue, M. T. Cicerone, and M. D. Ediger, *Macromolecules* **28**, 3425 (1995).
- ²³A. J. Bur and S. C. Roth, *Polym. Eng. Sci.* **44**, 805 (2004).
- ²⁴L. M. Smith, R. M. Weis, and H. M. McConnell, *Biophys. J.* **36**, 73 (1981).
- ²⁵M. T. Cicerone and M. D. Ediger, *J. Phys. Chem.* **97**, 10489 (1993).
- ²⁶J. Michl, E. W. Thulstrup, and J. H. Eggers, *Ber. Bunsenges. Phys. Chem.* **78**, 575 (1974).
- ²⁷R. Bergman, F. Alvarez, A. Alegria, and J. Colmenero, *J. Non-Cryst. Solids* **235**, 580 (1998).
- ²⁸D. Ehlich and H. Sillescu, *Macromolecules* **23**, 1600 (1990).
- ²⁹L. Goitiandia and A. Alegria, *J. Chem. Phys.* **121**, 1636 (2004).
- ³⁰R. A. Schapery, *Polym. Eng. Sci.* **9**, 295 (1969).